Penrose structures: Gap labeling and geometry

E. de Prunelé
Laboratoire de Physique Moléculaire, UMR CNRS 6624, Université de Franche Comté, 16 Route de Gray, La Bouloie, 25030 Besançon Cedex, France

(Received 14 February 2002; published 11 September 2002)

The electronic eigenvalues and eigenstates of finite parts of Penrose structures are studied on the basis of a recently proposed three-dimensional solvable model [J. Phys. A **30**, 7831 (1997)]. This model allows to take explicitely into account the geometry in three-dimensional space and involves no assumptions such as only nearest neighboring atoms coupling. For finite parts of a Penrose tiling, it is shown that the positions of some of the gaps in the integrated density of states are directly related to the geometry of the systems. As a result, the explicit expressions for ten gaps relative to infinite tilings are obtained from the known frequencies of vertex stars of Penrose tilings.

DOI: 10.1103/PhysRevB.66.094202 PACS number(s): 71.23.Ft, 71.20.−b

I. INTRODUCTION

Atoms located at vertices of a Penrose tiling[1] are models for two-dimensional quasicrystals.[2,3] The study of energy levels of these aperiodic structures has been the subject of intensive works.[4–37] Only three years after the publication of the experimental discovery of quasicrystals[38] in 1984, important reprints concerning electronic, phonon, and magnetic properties of quasicrystals were already collected in Chap. 7 of Ref. 39. At the end of the introductory remarks for this chapter, we quote ''it is our opinion that essentially nothing is known except special solutions for rather special models.'' Since that time, significant progress has been made, although some points remain controversial.[35] Nevertheless, concerning electronic spectrum for Penrose tilings, the quasitotality of subsequent works up to present day is based on tight-binding Hamiltonians $H=\Sigma_i \varepsilon_i |i\rangle\langle i| + \Sigma_{i,j} t_{ij} |i\rangle\langle j|$ where the *geometry* of the positions of the atoms in three-dimensional physical space is taken into account indirectly and not explicitly. Most of the works with these tight-binding Hamiltonians consider the case where only nearest neighboring atoms are coupled.

It is my opinion that these aperiodic model Hamiltonians indeed present a great mathematical and physical interest. It is also my opinion that results obtained with other models are necessary to help distinguish the properties that are generic from those which are not.

In a recent work,[40] the spectrum of finite subsystems of a Penrose tiling was considered on the basis of a model *with geometry in real three-dimensional space taken into account explicitly,* and *without any assumption of nearest neighboring atoms coupling*. This model was previously used for study of periodic[41] structures and is a particular case of a more general exactly solvable model.[42] The Hamiltonian is the sum of kinetic and interaction terms for an electron in three-dimensional physical space,

$$H=\frac{p^2}{2m}+\sum_{j=1}^{N} \lambda |\xi_j\rangle\langle\xi_j|, \tag{1}$$

$$|\xi_j\rangle = \exp(-i\mathbf{a}_j\cdot\mathbf{p}) r^{3/2} |r,0,0\rangle, \tag{2}$$

$$\langle r',l',m'|r,l,m\rangle = \frac{\delta(r'-r)}{r^2}\delta_{ll'}\delta_{mm'}, \tag{3}$$

$$\langle \mathbf{r}'|r,l,m\rangle = \frac{\delta(r'-r)}{r^2} Y_l^m(\mathbf{r}'). \tag{4}$$

The interaction is the sum of identical interactions each centered at the Penrose vertices. The interaction at center characterized by the vector position $\mathbf{a}_j$ is a separable one, with $|r,0,0\rangle \equiv |r,l=0,m=0\rangle$ an eigenvector of the squared orbital angular momentum with eigenvalue $l(l+1)$, an eigenvector of the component L_z of the orbital angular momentum with eigenvalue m, and a generalized eigenvector of the radial position operator with generalized eigenvalue r. Exact solutions for the energy eigenvalues and normalized eigenvectors can be obtained after numerical determination of the zeros of a determinant of a N order matrix (N is the total number of vertices) whose elements are simple analytic functions. The procedure for calculating these solutions is described in details in Refs. 42,41, and 40, and will not be repeated here.

The first results based on this model obtained in Ref. 40 for finite subsystems of a Penrose tiling clearly exhibit gaps in the integrated density of states (IDOS) but no theoretical interpretations were given.

The purpose of the present work is to show that these gaps are directly related to the geometry. As a result, the main gaps for infinite Penrose tilings are obtained analytically by extrapolation of results pertaining to finite subsystems.

It is very important to realize from start that this extrapolation procedure refers to the *point spectrum*. One *first* considers a finite system with boundary conditions corresponding to wave functions exponentially decreasing *at infinity*, and *then* one considers the limit where the size of the system tends to infinity in all directions. It is recalled that z belongs to the point spectrum if the operator $(z-H)$ has no inverse, to the continuous spectrum if the operator $(z-H)$ has an inverse not bounded with dense domain, and to the residual spectrum if the operator $(z-H)$ has an inverse with domain not dense. see, e.g., Ref. 43. This procedure is clearly relevant to the study of real physical systems. It avoids the introduction of periodic boundary conditions, or of periodic approximants that, in my opinion, may be useful, but can be avoided as shown by the present work. In particular, a wave vector $\vec{k}$ is essentially a label for one irreducible representa-

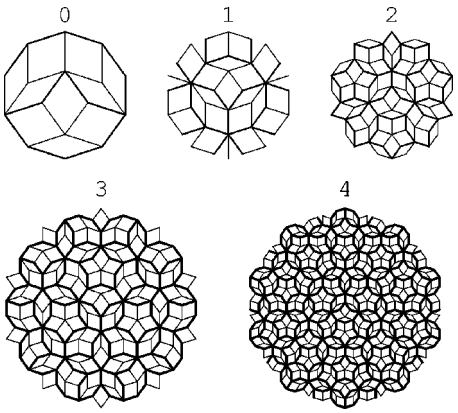

FIG. 1. The five systems (not to scale).

tion of a translation group, and therefore the consideration of these wave vectors $\vec{k}$ is intrinsically related to the use of periodic approximants and is not an unavoidable tool for analyzing infinite systems that are not periodic.

II. GEOMETRICAL INTERPRETATION OF THE MAIN GAPS

The finite systems that will be considered here are numbered 0,1,2,3,4 (Fig. 1). The system $i+1$ is obtained by deflating the system i and then rescaling it by multiplying all distances by the golden ratio $\tau=(1+\sqrt{5})/2$ [symbolically $i+1=\tau D(i)$]. Thus all the five systems have the same length for an edge of a rhombus in the forthcoming calculations of the spectrum. The total numbers of vertices N_i for each system is $N_0=16$, $N_1=36$, $N_2=76$, $N_3=186$, $N_4=476$. For comparison with the results obtained in Ref. 40, the same values of the interaction parameters have been chosen,

$$\lambda=-0.398\,909 \text{ a.u.}, \tag{5}$$

$$r=1.817\,6943 \text{ a.u.}, \tag{6}$$

$$c=6.0816 \text{ a.u.}, \tag{7}$$

c is the common length of the edge of Penrose rhombi. The original choice for these values was motivated by the description of band structure of lithium crystal,[41] but these values are not critical and some calculations made with other values lead to the same conclusions that are presented below.

The system 0 has been chosen because its form, a regular decagon, has a low perimeter to surface ratio, in order to minimize boundary effects. The five systems have a vertical axis as symmetry axis to be called the y axis in the following.

Figure 1 describes the systems 0,1,2,3,4 (with an arbitrary scaling for each system). The edges are drawn for better visualization, but the eigenvalues and eigenvectors of the Hamiltonian depends only on the vertices positions. It can be shown that the Penrose two prototiles tilings are in bijective correspondence with the tilings, thereafter to be denoted type I tilings, constructed from three prototiles depicted in Fig. 2 and called the ''star,'' the ''boat,'' and the ''cigar.'' A direct proof, based on the listing of all the vertex stars of a Penrose

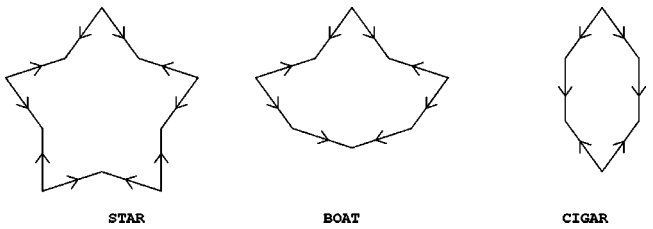

FIG. 2. The three prototiles for type I tilings.

tiling, is given in the Appendix. This appendix also contains some definitions and results that will be used here.

A word of caution: the word *star* alone refers to one of the three above prototiles, and should not be confused with the word star in the expression *vertex star* $(at\ p)$ which refers to the usual definition given in the Appendix.

The contours of these three prototiles have been underlined in Fig. 1 for the sake of simplifying the interpretation of the spectra. The Penrose vertices internal to these three prototiles will be called *internal vertices*, the vertices of these three prototiles (the other Penrose vertices) will be called *external vertices*. It should be noted that the method of projection from a higher dimensional lattice naturally distinguishes external from internal vertices.[44] An important property is that the external vertices of a Penrose tiling P are the internal vertices of the deflated tiling $D(P)$ (See Appendix).

For the discussion in this paragraph, the units of distance will be taken to be the common length c given by Eq. (7) for all edges of all rhombi of all systems. With this choice of units, Eq. (7) reads $c=1$.

It is very important for the sequel to notice from the start that, *for an infinite tiling*, the short diagonals (length $1/\tau$) of a thin rhombus always appear inside a cigar or a boat. They always appear with a common vertex in a cigar, whereas they always appear isolated in a boat. This is important because the distance between two *nearest neighbors* vertices is either 1 or $1/\tau$. Two vertices separated by the shortest distance $1/\tau$ thus are always inside or on the boundary of a cigar or a boat. Hereafter, a vertex with a neighboring vertex at distance $1/\tau$ will be called a vertex of type A, a vertex with a nearest neighboring vertex at distance 1 will be called a vertex of type B. To distinguish between the vertices of type A which belong to a cigar and those which belong to a boat, we add a subscript: A_c for cigar, A_b for boat.

The five exact point spectra computed numerically are reported in Fig. 3 in the form of unnormalized integrated density of states (UIDOS) plots. Specifically, the energy eigenvalues are numbered in increasing order starting with unity. The horizontal axis is the energy, the vertical one reports the running number of the eigenvalues. The total number of linearly independent states is equal to the total number of vertices and to the total number of energy eigenvalues as no degeneracy occurs. It is seen by comparison with Ref. 40 that the behavior of the UIDOS is the same that was found in Ref. 40 for different geometrical systems. This fact, together with the consideration of much larger systems in the present paper is a first indication that finite-boundary effects seem not to play an essential role.

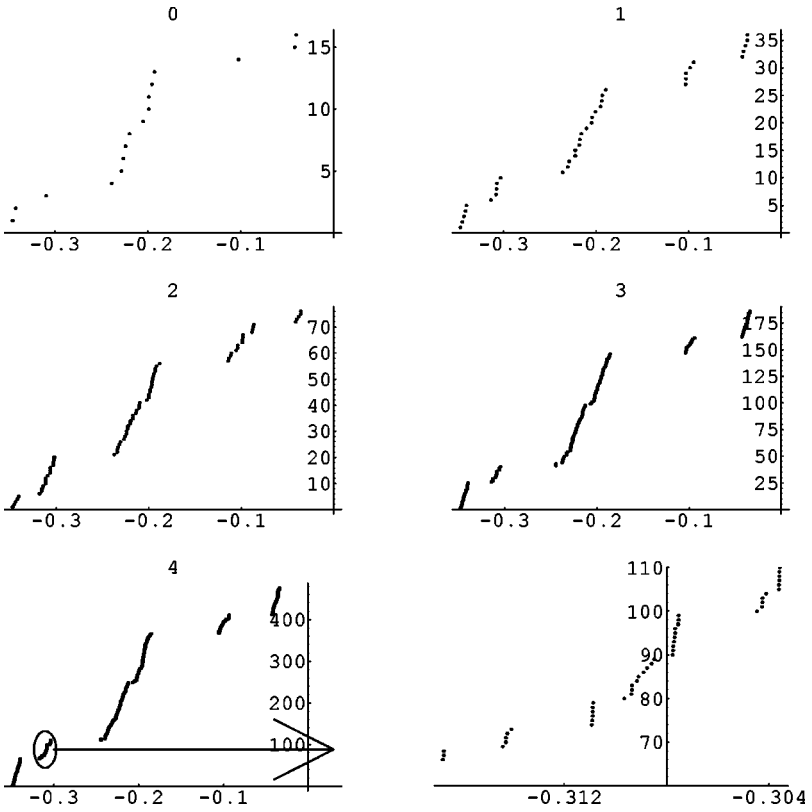

FIG. 3. Unnormalized integrated density of states for the five systems. The last graph is an enlarged view of part of the last but one. The abscissa axis represents the energy. The ordinate axis represents the running numbers of states ordered according to increasing energy (see text).

A. Analysis of the contour plots for the system 0

The contour plots for all the wave functions evaluated in the plane of the systems, associated with these energy eigenvalues have been drawn and analyzed for most of all the eigenstates of the five systems. This analysis gives the key for the interpretation of the gaps in the DOS. Of course, we cannot report all these contour plots, but Fig. 4 displays all contourplots for the system 0.

There are ten equally spaced contours between the extrema values, and, for each of the 16 graphs, the shading corresponding to nearly zero values of the wave function is the one present at the corners (where the wave function is exponentially decreasing). The vertices i where the wave function Ψ has the most important weights $\langle \xi_i | \Psi \rangle$ will be characterized explicitly in the text below.

Much can be learned from the contour plots of Fig. 4.

First, the states of lowest energy (states 1,2) have a wave function with important weights on the vertices belonging to the two short diagonals inside a cigar. These wave functions are *approximately locally completely symmetric* (i.e., they have a constant sign on each of the two short diagonals of the cigar, and this sign is the same). The wave function of state 1 (ground state) has a constant sign, the one of state 2 is antisymmetric with respect to the y axis. The states of highest energy (states 15,16) have also a wave function with important weights on the vertices belonging to the two short diagonals inside a cigar. These wave functions are *approximately locally completely antisymmetric* (i.e., they change signs inside each of the two thin rhombi of a cigar, the lines of nodes being roughly perpendicular to the two short diagonals inside the cigar). The wave function of state 15 is symmetric with respect to the y axis, the one of state 16 antisymmetric.

Second, the following state of lowest energy (state 3) has a wave function with important weights on the vertices belonging to an isolated short diagonal. This wave function is

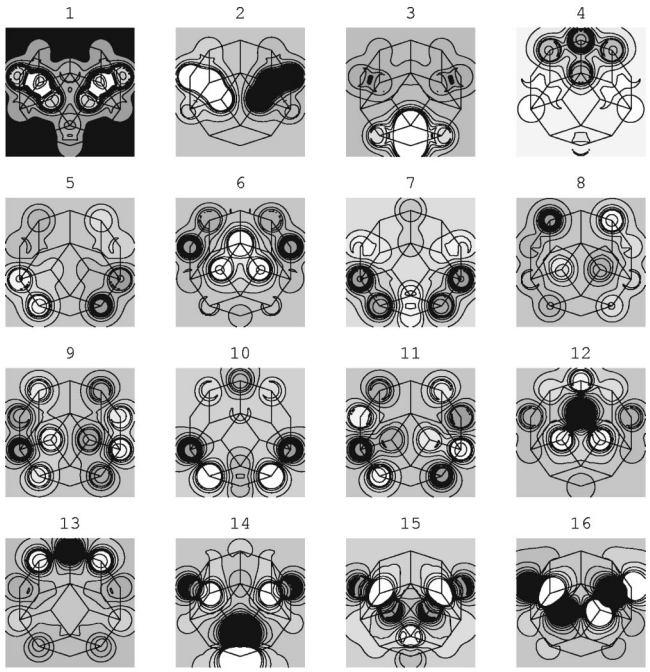

FIG. 4. Contour plots of the 16 eigenfunctions for the system 0.

approximately locally symmetric (i.e., has a constant sign on the short diagonal inside the boat). The preceding state of highest energy (state 14) has also a wave function with important weights on the vertices belonging to an isolated short diagonal. This wave function is *approximately locally antisymmetric* (i.e., it changes sign inside the thin rhombus of the boat).

Third, the following state of lowest energy (state 4) has a wave function with important weights centered on the vertices, which form the region of highest concentration of vertices of type B (four vertices near the top of the system). This wave function is *approximately locally completely symmetric* (i.e., has a constant sign in a region surrounding the four vertices). The preceding state of highest energy (state 13) has also a wave function with important weights centered on the vertices, which form the region of highest concentration of vertices of type B. This wave function is *approximately locally completely antisymmetric* (i.e., has alternating sign between two consecutive vertices. From geometrical considerations, this is possible only if the weight on one of the four vertices is close to zero, which is indeed the case).

It remains to discuss the eight middle energy states 5,6, . . . ,12. It can be seen that states 5 to 9 are locally symmetric (i.e., there are two vertices of type B separated by unit distance where the wave function has important weights, and the wave function does not change sign between these two vertices). The state 8 is included here somewhat arbitrarily since there are no two vertices of type B separated by unit distance where the wave function has important weights. Then follow the states 10 to 12: they are locally antisymmetric (i.e. there do not exist two vertices of type B separated by unit distance where the wave function has important weights, and the wave function does not change sign between these two vertices).

Finally, a last comment. The six vertices of type A_c lead only to four states (1,2,15,16) located at both the extremities of the spectrum. Two vertices of type A_c thus contribute significantly to states with energy not in the two extrema regions. The spectrum associated with the system consisting of only three vertices disposed at the vertices A_c of a cigar has three eigenvalues, the lowest one yielding a state having the local symmetry of states 1,2, the highest one yielding a state having the local symmetry of states 15,16, the middle one having a line of nodes separating the two external vertices (the internal one is the vertex shared by the two short diagonals). These two external vertices are separated by a distance greater than one. Thus, to interpret the whole spectrum, one can proceed as follows.

One first considers the subsystem consisting of only vertices of type A_c. One requires that the three vertices of type A_c of a cigar contribute only to states having no nodes in the middle region separating the two external vertices. One thus interprets the two extrema regions of the spectrum (1,2,15,16). One then considers the subsystem consisting only of vertices of type A_b. One thus interprets the last but one extremity region of the spectrum (3,14). One finally considers the subsystem consisting only of vertices of type B and A_c, but one requires that the three vertices of type A_c of a cigar contribute only to states having a line of nodes in the middle region separating the two external vertices. One thus interprets the middle region of the spectrum (4,5, . . . ,13).

B. Geometrical interpretation of the four main gaps for the five systems and extrapolation to infinite systems

Let us call the normalized integrated density of states (NIDOS) the IDOS which takes the value unity when the energy is greater than or equal to the largest energy eigenvalue, and takes the value zero when the energy is lower than the lowest energy eigenvalue. If we apply the conclusions of the preceding analysis to the five systems, the four main gaps in the NIDOS should be given by the geometrical ratios reported in the first line of Eq. (8), where N is the total number of vertices, n_c is number of pairs of short diagonals sharing a common vertex, n_b is the number of isolated short diagonals.

System	$\frac{n_c}{N}$	$\frac{N-n_c}{N}$	$\frac{n_c+n_b}{N}$	$\frac{N-n_c-n_b}{N}$
0	$\frac{2}{16}=\frac{1}{8}$	$\frac{16-2}{16}=\frac{7}{8}$	$\frac{2+1}{16}=\frac{3}{16}$	$\frac{16-2-1}{16}=\frac{13}{16}$
1	$\frac{5}{36}$	$\frac{36-5}{36}=\frac{31}{36}$	$\frac{5+5}{36}=\frac{5}{18}$	$\frac{36-5-5}{36}=\frac{13}{18}$
2	$\frac{5}{76}$	$\frac{76-5}{76}=\frac{71}{76}$	$\frac{5+15}{76}=\frac{5}{19}$	$\frac{76-5-15}{76}=\frac{14}{19}$
3	$\frac{25}{186}$	$\frac{186-25}{186}=\frac{161}{186}$	$\frac{25+15}{186}=\frac{20}{93}$	$\frac{186-25-15}{186}=\frac{73}{93}$
4	$\frac{65}{476}$	$\frac{476-65}{476}=\frac{411}{476}$	$\frac{65+45}{476}=\frac{55}{238}$	$\frac{476-65-45}{476}=\frac{183}{238}$
∞	τ^{-4} $=5-3\tau$ $\simeq 0.145898$ A	$1-\tau^{-4}$ $=-4+3\tau$ $\simeq 0.854102$ D	$\tau^{-4}+\tau^{-5}$ $=-3+2\tau$ $\simeq 0.236068$ B	$1-\tau^{-4}-\tau^{-5}$ $=4-2\tau$ $\simeq 0.763932$ C

(8)

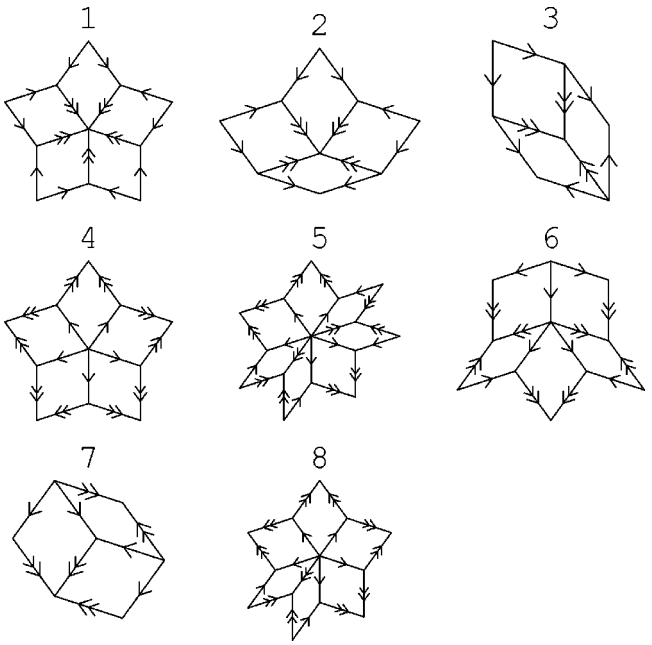

FIG. 5. The eight vertex stars of a Penrose tiling.

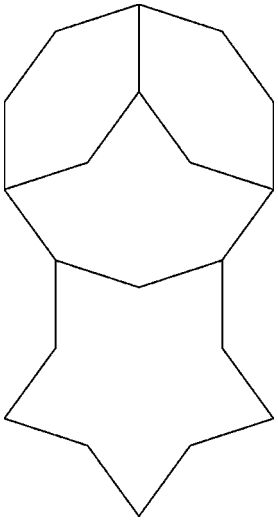

FIG. 6. An ubiquitous pattern for type I tilings.

If we now compare these values deduced from Fig. 1, i.e., from pure geometry, to the gap values deduced from the energies reported in Fig. 3, i.e., from exact quantum computations, one obtains *perfect agreement*. (This may be difficult to see from the only Fig. 3 but we stress that the agreement is exact for all the twenty numbers.) This leads us to extrapolate to infinity with confidence and the results of this extrapolation are reported in the last line of Eq. (8). The values in the last line of Eq. (8) are obtained by noting that, for an infinite tiling, n_c/N is the frequency of vertex star of type 3, n_b/N is the frequency of vertex star of type 2 (see Fig. 5). The frequencies of these vertex stars are known and are derived in the Appendix [see Eq. (A1)] for the sake of completeness.

These main gaps will be called A, B, C, D in order of increasing energy from now on.

III. GEOMETRICAL INTERPRETATION AND DETERMINATION OF OTHER GAPS FOR INFINITE SYSTEMS

The success of the previous geometrical interpretation for the first four main gaps encourages further geometrical gap determinations. We presently have not determined a general formula for all the gaps. The purpose of this paragraph is to determine geometrically some of them whose interpretation is particularly simple. The interest is to illustrate the importance of what could be called a renormalization procedure, whose quantitative implementation relies upon the inflation-deflation properties of Penrose tilings.

A. Secondary gaps between gaps A and B

Let us first consider the states situated between the first, τ^{-4}, and second, $\tau^{-4}+\tau^{-5}$, main gaps A and B.

We shall determine gaps relative to infinite system with the help of the gap relative to system 4. The UIDOS for this region is enlarged in the last graph of Fig. 3. *In this energy region*, the number of linearly independent states is equal to the number of short isolated diagonals. We have seen that a boat is in bijective correspondence with an isolated short diagonal for infinite Penrose tiling. It has also be seen in the Appendix that a boat always meets a star according to Fig. 6. It can then be shown that the isolated short diagonals can be grouped to form the figures of a star surrounded by 5, 3, or 1 boats (to be denoted S_{b5}, S_{b3}, S_{b1}). Specifically, a star with inner vertex p of tiling P gives for $D^2(P)$ a star with inner vertex p surrounded by five boats, a boat with inner vertex p of tiling P gives for $D^2(P)$ a star with inner vertex p surrounded by three boats, a cigar with inner vertex p of tiling P gives for $D^2(P)$ a star with inner vertex p surrounded by one boat. For an illustration, see Fig. 7, where the system 2 and the system $D^2(2)$ (system 4 without rescaling by τ^2) are displayed together (without inner vertices).

To follow the deduction, it is important now to localize in the last graph of Fig. 1 or in Fig. 7, the three stars surrounded by five boats, the five stars surrounded by three boats, the five stars surrounded by one boat, and finally the ten isolated short diagonals on the boundary. This gives a total of $3\times5+5\times3+5+10=45$ isolated short diagonals that have to be related to the 45 linearly independent states 66 to 110 (of course, not a direct correspondence).

The locally totally symmetric states of S_{b5} should then give a gap at $\tau^{-4}+x$ where x is the frequency of a star surrounded by five boats. This frequency x can be determined, for example, by noting that it is equal to the frequency of the inner vertices f_i [Eq (A2)] divided by τ^8 since the inner vertices of P are the centers of stars surrounded by fives boats of $D^4(P)$ (see Appendix). One thus predicts a gap at $\tau^{-4}+(3-\tau)/5\,\tau^8=(148-91\tau)/5\simeq0.151\,781$.

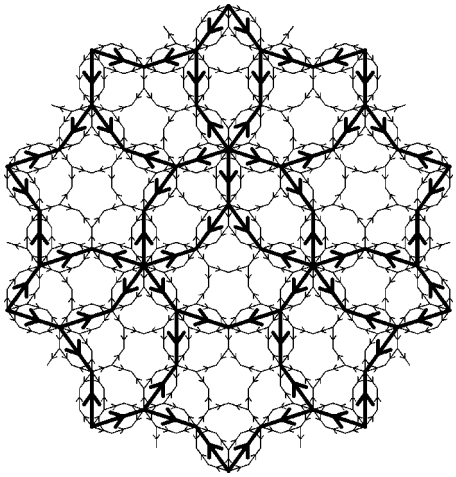

FIG. 7. Two Penrose deflations of type I tiling.

This result can be obtained in another way by noting that the *relative* frequencies of S_{b5}, S_{b3}, S_{b1} are given by Eq. (A3) in that order due to the relation between P and $D^2(P)$, which has been discussed above. The locally totally symmetric states of S_{b5} should then give a gap at $\tau^{-4}+\alpha\tau^{-4}$ with α solution of

$$\tau^{-5}=\alpha\left(5\tau^{-4}+3\frac{\tau^2+1}{\tau^5}+1\frac{\tau^2+1}{\tau^4}\right).$$

The left-hand side represents the variation range of the NIDOS in the energy region considered, the right-hand side represents the number of short isolated diagonals. As the solution is $\alpha=(18-11\tau)/5$, one thus recovers the gap value $(148-91\tau)/5$.

This interpretation is confirmed, for example, by a closer look at the spectrum of system 4 in the concerned energy range. System 4 has three stars surrounded by five boats. One sees in Fig. 3 a gap after three levels (with numbers 66, 67, 68). The corresponding three states have strong components on the vertices of the isolated short diagonals of the three S_{b5}. Figure 8 shows a countour plot of the wave functions of these states. The conventions for contour levels and shading are the same as the ones for Fig. 4. The wave functions indeed take most significant values in the regions of the stars surrounded by five boats. (Compare Fig. 8 with the last graph of Fig. 1.)

Similarly, the next five states 69, 70, 71, 72, and 73 have wave functions with dominant weight on the vertices of the short diagonals belonging to the five stars surrounded by three boats of system 4. The locally totally symmetric states of S_{b3} should then give a gap at $(148-91\tau)/5+\alpha(\tau^2+1)/\tau^5=(-127+79\tau)/5\simeq 0.164\,937$.

The next six states, 74 to 79, and the last six states 105 to 110 have wave functions with dominant weights on the vertices of the short diagonals belonging to the three stars surrounded by five boats. A star surrounded by five boats has the local symmetry group D_{5h} whose inequivalent irreducible representations are of dimension 1 or 2. On the other hand, a star surrounded by five boats should give five linearly independent states that are locally symmetric on the short diagonals. One has already been taken into account (the locally totally symmetric state of S_{b5}). There remain four, which we attribute to irreducible representations of dimension 2. One therefore has a gap at $(-127+79\tau)/5+2(3-\tau)/5\tau^8=(119-73\tau)/5\simeq 0.176\,704$ and another one at $\tau^{-4}+\tau^{-5}-2(3-\tau)/5\tau^8=[9(-29+18\tau)]/5\simeq 0.224\,301$.

The five states 100 to 104 have wave functions with dominant weights on the vertices of the short diagonals belonging to the five stars surrounded by three boats. One thus expects a gap at $[9(-29+18\tau))/5-\alpha(\tau^2+1)/\tau^5=(9(-29+18\tau))/5-(18-11\tau)/5(-11+7\tau)=(2(7-4\tau))/5\simeq 0.211\,46$.

Among the $5\times 3=15$ linearly independent states related to the five stars surrounded by three boats, 5×2 have been attributed. It remains $[(110-66)+1]-(3+5+6+6+5)=20$ states unattributed, i.e., the states numbered 80 to 99. These states either have wave functions with dominant weights on the vertices of the short diagonals belonging to the five stars surrounded by three boats, or wave functions with dominant weights on the vertices of the short diagonals belonging to the five stars surrounded by one boat, or dominant weights on the vertices of the ten isolated short diagonals located at the boundary. There is no a clear ordering between states with wave functions with dominant weights on the vertices of the short diagonals belonging to the five stars surrounded by three boats and the other ones in this energy region probably due to the boundary effects, i.e., due to the presence of the ten isolated short diagonals at the boundary. So we shall consider these 20 states globally and shall not try to determine the position of the gap between them.

To summarize, five gaps between gap A and B of system 4 have been extrapolated for infinite tiling as follows.

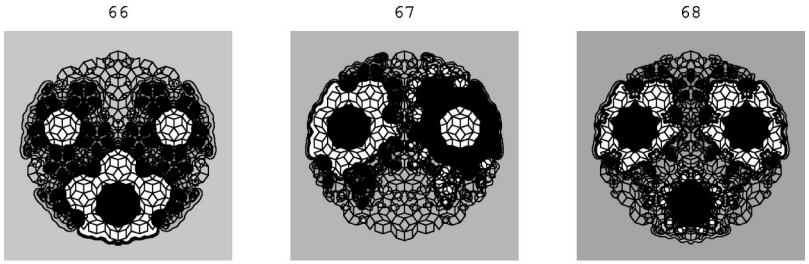

FIG. 8. Contour plots for wave functions 66,67,68 of system 4.

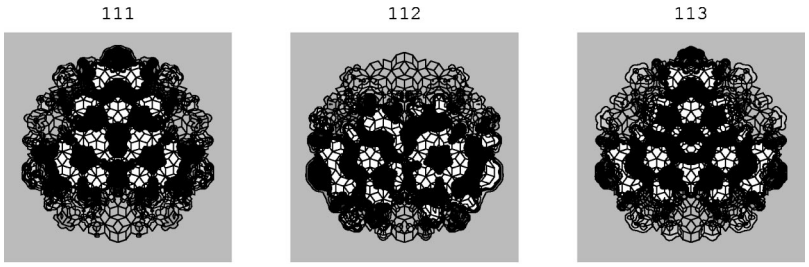

FIG. 9. Contour plots for wave functions 111,112,113 of system 4.

$$\begin{array}{lccccc} \text{System 4} & \frac{68}{476} & \frac{73}{476} & \frac{79}{476} & \frac{99}{476} & \frac{104}{476} \\ & \frac{148-91\tau}{5} & \frac{-127+79\tau}{5} & \frac{119-73\tau}{5} & \frac{2(7-4\tau)}{5} & \frac{9(-29+18\tau)}{5} \\ \infty & & & & & \\ & \simeq 0.151781 & \simeq 0.164937 & \simeq 0.176704 & \simeq 0.211146 & \simeq 0.224301 \end{array} \tag{9}$$

B. First secondary gap after B

The states between gaps B and C are all those that have no predominant weights on the two vertices of a short diagonal (isolated or not). It is therefore expected that the wave functions of the lowest energy states are concentrated near the greatest local density of vertices separated by units (i.e., the length edge of a rhombus, 6.0816 a.u. in the numerical application). These greatest local density of vertices are centered on vertices p with Penrose vertex star at p of type 4 (See Fig. 5). They correspond to the intersection of five cigars at a common vertex. There are three such configurations in system 4 and there are indeed three states after gap B and before the first secondary gap after B (this secondary gap is almost visible on graph 4 of Fig. 3). The contourplots of these states, within the same conventions as for Fig. 4 and Fig. 8, are reported in Fig. 9. These locally symmetric states have dominant weights on the three groups of six vertices consisting of the central Penrose vertex of type 4 surrounded by five vertices at units distance of this central vertex. (Compare Fig. 9 with the last graph of Fig. 1). As the frequency of Penrose vertex stars at p of type 4 is $\tau^{-5}/(\tau^4-1)=(47-29\tau)/5$, the position of the secondary gap is $\tau^{-4}+\tau^{-5}+\tau^{-5}/(\tau^4-1)=$

$$\frac{32-19\tau}{5}\simeq 0.251\,471. \tag{10}$$

IV. CONCLUSION

This work has provided clear evidence that gap labeling should be related to geometry only. We have obtained ten explicit expressions for positions of gaps [see Eqs. (8), (9), and (10)]. The reason for the choice for these ten particular gaps is simply that they appear to us as the easiest ones to determine. To my knowledge, only one gap position has been previously published,[35] $(-2+4\tau)/5\simeq 0.894\,427$ in the framework of tight-binding Hamiltonians. This gap is after the four main gap D we have found at $4-2\tau$ [see Eq. (8)]. Figure 10 shows an enlarged view of the UIDOS for system 4 after this four main gap D. It is seen on this figure that this energy region appears *a priori* more difficult to interpret, but $(-2+4\tau)/5\times 476\simeq 425.747$ in quite compatible with, for example, a gap at 430 or 427 for the finite system 4.

The present gap determinations were done in a logical, but rather pedestrian, way. Other particular geometrical gap determinations could be performed along the same way, but we are presently looking for a more systematic way, and for general formula.

The guiding principles should be the following.

(1) Local approximated symmetry and local approximated orthogonality of states.

(2) Renormalization procedure: The states characterized by the same local properties [characteristic length and given local (at this characteristic length) symmetry] have to be considered (for the purpose of counting only, not for the determination of energy or eigenfunctions) independent of the states characterized by a different local property, and then group together in ''packets'' of different symmetries and the procedure is repeated at the scale of these packets. The quantitative exploitation of this renormalization procedure relies upon the inflation-deflation properties of Penrose tilings. The difficulties stem from the fact that the centers of these packets may not form the vertices of a Penrose tiling but be only

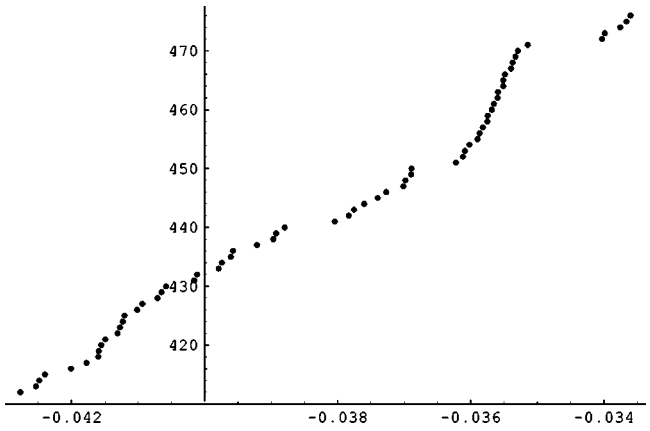

FIG. 10. Enlarged view of the highest energy region of the UIDOS of system 4 (see Fig. 3).

proper subsets, for example, the internal or external vertices. Difficulties could also arise because the same region of energy could accidentally involve states of different local properties.

A justification of these guiding principles from first principles of quantum mechanics should be based on the two general results: variational principle and orthogonality of states belonging to different eigenvalues of an Hermitian Hamiltonian.

If a geometrical procedure analogous to the one we have described in this paper can indeed be repeated indefinitely in all energy ranges, we reach two general conclusions.

A wave function on a (infinite) Penrose tilings could not be localized in a finite volume (i.e., its modulus cannot always decrease exponentially outside a finite volume).

The geometrical determination of the positions of the gaps leads to expression of the form $a+b\tau$ with a and b rationals. (The present results are of the form $(n+m\tau)/5$ with n,m integers)

To recast our results concerning wave functions within the usual terminology used in the studies based on a tight-binding Hamiltonian, we would qualify the wave functions as *critical*: localized at distinct local patterns, but extended over the whole lattice.[33] No evidence for the existence of strong confined states has been found.

The nature of the spectrum clearly manifests a fractal structure, at least on some energy ranges, which has to be related to both local symmetry and Convay theorem[48] about the infinitely many occurrences of any allowed finite configurations in an infinite tiling. Our results are compatible with the prediction of gap labeling rules.[49,50]

ACKNOWLEDGMENTS

The author acknowledges helpful discussions with X. Bouju.

APPENDIX: PENROSE TILINGS AND TYPE I TILINGS

Portions of tilings involving the geometrical shapes of the three prototiles presented in Fig. 2, appear sometimes in the literature (See, e.g., Refs. 14,45,46). To my knowledge, no claim and proof that these three prototiles tile the plane and tile it only aperiodically, and that there is a bijection between the set of such tilings and the set of Penrose tilings by two rhombi[1] have been published. Although the proof is rather elementary, it is presented in the Appendix for the sake of completeness and also for introducing some definitions and results used in this paper.

To distinguish the Penrose tilings constructed from two rhombi,[1] from the tilings constructed from the three prototiles of Fig. 2, these latter tilings are referred as type I tilings.

Proposition 1. All the tilings of type I are derived from the Penrose tilings with two rhombi simply by selecting the one arrow edges of these tilings.

For an illustration, see Figs. 1 or 7. A proof of this proposition follows after two definitions and five elementary properties. The first definition is the usual one (See, e.g., Ref. 2):

Definition 1. Let T be a tiling. The *vertex star* $W(v)$ at a vertex v of T is the set of all tiles in T that meet v.

A second definition relative to Penrose tilings with rhombi will be needed. First, we precise what we mean by the term angle: two edges meeting at a vertex determine *two* (positive) angles (whose sum is 2π).

Definition 2. An angle between two single-arrow edges meeting at a vertex v, with no single-arrow edge (with vertex v) interior to this angle will be called *a single-arrow angle* at that vertex.

The Fig. 5 presents the atlas of globally legal vertex stars of Penrose tilings (See, e.g., Ref. 2), hereafter referred as vertex stars of types 1 to 8. Five properties are immediate by inspection.

Property 1. Only vertex stars of types 1,2,3 have the following properties: only single-arrow edges on their boundary, and no single-arrow edge in their interior.

Property 2. All the vertex stars $W(v)$ of types 4,5,6,7,8 do not have two double-arrow edges meeting at v with an angle of $2\pi/5$.

Property 3. All the vertex stars $W(v)$ of types 4,5,6,7,8 do not have two double-arrow edges meeting at v with an angle of $4\pi/5$ *and* no single-arrow edge (with vertex v) in the interior of this angle.

Property 4. All the vertex stars $W(v)$ of types 4,5,6,7,8 do not have three double-arrow edges meeting at v.

Property 5. The single-arrow angles at a vertex v of a vertex star at v necessarily are of one among the following five types.

(1) An angle equal to $2\pi/5$ and no double arrow in its interior (vertex stars of types 4,5,6,8)

(2) An angle equal to $4\pi/5$ and no double arrow in its interior (vertex stars of type 7)

(3) An angle equal to $2\pi/5$ and a double arrow in its interior (vertex stars of types 5,8)

(4) An angle equal to $4\pi/5$ and a double arrow in its interior (vertex stars of type 6)

(5) An angle equal to $6\pi/5$ and a double arrow in its interior (vertex stars of type 7).

Now the proof of proposition **1**.

Consider an arbitrary given Penrose tiling. In this tiling, select all vertex stars $W(v)$ of types 1,2,3. Remove in all the selected vertex stars $W(v)$ the vertex v and also the double-arrow edges meeting at v. The selected vertex stars have thus been replaced by one of the three prototiles of Fig. 2. None of these prototiles overlaps because if two of them overlap, the single-arrow edge on the boundary of one would be an inner single-arrow edge of the initial Penrose vertex stars corresponding to the other, and the selected vertex stars 1,2,3 have no inner single-arrow edge by property 1. Either the set of these three prototiles tile the plane, or not. If they do, the proposition is true for the tiling considered. If not, there remains at least one vertex star at a vertex v_0, of type belonging to the set 4,5,6,7,8 and with v_0 not belonging to the boundary of one of the three prototiles of Fig. 2. Then consider all the possible single-arrow angles at the vertex v_0.

A single-arrow angle of type 1 at the vertex v_0 necessarily belongs to a thick rhombus as can be seen by inspection of

the vertex star of types 4,5,6,8 on Fig. 5. The vertex v' where the two double-arrow edges of this thick rhombus meet necessarily has a vertex star $W(v')$ at v' of types 1,2,3 by property 2.

A single-arrow angle of type 2 at the vertex v_0 necessarily belongs to a thin rhombus as can be seen by inspection of the vertex star of type 7 on Fig. 5. The vertex v' where the two double-arrow edges of this thin rhombus meet necessarily has a vertex star $W(v')$ at v' of types 1,2,3 by property 3.

A single-arrow angle of type 3 at the vertex v_0 determines a vertex v' at the other extremity of the double-arrow edge. At this vertex, three double-arrow edges meet as seen from vertex star 8 on Fig. 5. Therefore, by property 4, the vertex v' necessarily has a vertex star $W(v')$ at v' of types 1,2,3.

A single-arrow angle of type 4 at the vertex v_0 determines a vertex v' at the other extremity of the double-arrow edge. At this vertex, three double-arrow edges meet as seen from vertex star 6 on Fig. 5. Therefore, by property 4, the vertex v' necessarily has a vertex star $W(v')$ at v' of types 1,2,3.

A single-arrow angle of type 5 at the vertex v_0 determines a vertex v' at the other extremity of the double-arrow edge. At this vertex, three double-arrow edges meet as seen from vertex star 7 on Fig. 5. Therefore, by property 4, the vertex v' necessarily has a vertex star $W(v')$ at v' of types 1,2,3.

Thus, all the above vertices v' [which are on the boundary of the vertex star $W(v_0)$ at the vertex v_0], have vertex star $W(v')$ of types 1,2,3. As a result, the vertex v_0 belongs to the boundary of one of the three prototiles of Fig. 2, contrary to the initial supposition. This proves that each Penrose tiling gives a unique type I tiling. It remains to prove that all type I tilings can be obtained in this way. Thus consider an arbitrary type I tiling. It is clear by considering the Fig. 2 that there is one and only one way to add a vertex into the star, the boat, and the cigar, (and double-arrow edges inside these three prototiles) so that the star is transformed into a Penrose vertex star of type 1, the boat into a Penrose vertex star of type 2, the cigar into a Penrose vertex star of type 3. This concludes the proof of proposition 1.

An important property is the composition property: a type I tiling can be uniquely inflated and uniquely deflated. This is illustrated in Fig. 11 for one deflation and in Fig. 7 for two deflations.

For a better visualization of type I tiling, it is useful to note that a boat automatically forces the configuration presented in Fig. 6. This can be proved by successive trials with the prototiles of Fig. 2. An indirect proof is as follows: Fig. 7 shows that, in a deflation of each of the three prototiles, a boat always appears with the configuration presented in Fig. 6. By successive deflations, one can thus obtained a connected region with an arbitrary large number of prototiles, where the boat only appears in the configuration of Fig. 6. It is a known property of Penrose tiling that every local (globally legal) configuration must appear as the number of tiles increases. Thus the configuration of Fig. 6 is the only possible one.

1. Frequencies

The frequency of the eight different vertex stars of a Penrose tiling can be determined from the method of projection from higher dimensional lattices.[44] It can also be obtained, together with the relative frequency of the two rhombi, by considering an infinite sequence of deflations, as described in Ref. 47. For the sake of self-consistency, this last method is now rapidly summarized. The two rhombi together with the eight vertex stars are considered as ten objects, numbered 1 for the thick rhombus, 2 for the thin rhombus, and $j+2$ for the vertex stars with j the number reported in Fig. 5. The vertex stars at p of a Penrose tiling P are also vertex stars at p of the deflated tiling $D(P)$. There are in addition other vertex stars in $D(P)$. Among them, those that are inside a thick rhombus T of P are qualified to be generated by T. Those that are not inside a thick rhombus T of P are necessarily on an edge shared by a thick rhombus T and are qualified to be generated by T, with a factor one half. One then has the substitution matrix

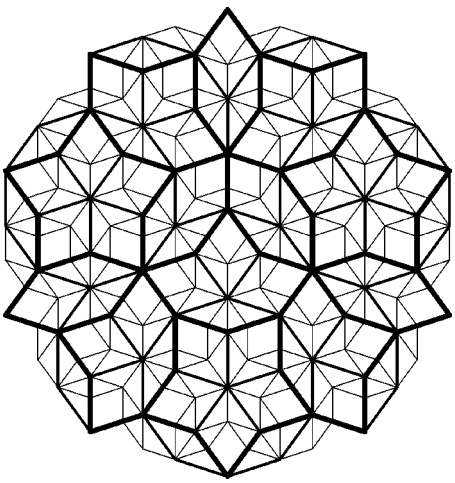

FIG. 11. One Penrose deflation of system 2, i.e., system 3 unscaled with respect to system 2.

$$\begin{pmatrix} 2 & 1 & 0 & 0 & 0 & 0 & 0 & 0 & 0 & 0 \\ 1 & 1 & 0 & 0 & 0 & 0 & 0 & 0 & 0 & 0 \\ 0 & 0 & 0 & 0 & 0 & 1 & 1 & 0 & 0 & 1 \\ 0 & 0 & 0 & 0 & 0 & 0 & 0 & 1 & 0 & 0 \\ 0 & 0 & 0 & 0 & 0 & 0 & 0 & 0 & 1 & 0 \\ 0 & 0 & 1 & 0 & 0 & 0 & 0 & 0 & 0 & 0 \\ 0 & 0 & 0 & 0 & 1 & 0 & 0 & 0 & 0 & 0 \\ 1 & 0 & 0 & 0 & 0 & 0 & 0 & 0 & 0 & 0 \\ 1 & 1 & 0 & 0 & 0 & 0 & 0 & 0 & 0 & 0 \\ 0 & 0 & 0 & 1 & 0 & 0 & 0 & 0 & 0 & 0 \end{pmatrix}.$$

For example, a thick rhombus T of P is considered to be the parent of two thick rhombi of $D(P)$, one thin rhombus of $D(P)$, one vertex star of type 6, and one vertex star of type 7. This gives the first column of the substitution matrix. The greatest eigenvalue of this matrix is τ^2, and its column eigenvectors are proportional to

$$\left(\tau^6 \tau^5 \frac{\tau^4}{\tau^4-1} \tau^2 \tau^3 \frac{\tau^2}{\tau^4-1} \tau \tau^4 \tau^5 1 \right)^t.$$

The two first components tell us that the frequency of the thick rhombus is equal to τ times the frequency of the thin rhombus. It is convenient for the sequel to normalize the frequencies of the vertex stars only (i.e., not including the objects rhombi) to unity. This amounts to dividing the eight last components by τ^7.

1	2	3	4	5	6	7	8
$\frac{\tau^{-3}}{\tau^4-1}=\frac{18-11\tau}{5}$	τ^{-5}	τ^{-4}	$\frac{\tau^{-5}}{\tau^4-1}=\frac{47-29\tau}{5}$	τ^{-6}	τ^{-3}	τ^{-2}	τ^{-7}

(A1)

The vertex star numbers reported in Fig. 5 are in the first line, the sum of the corresponding frequencies in second line is equal to unity. It will be useful for the sequel to determine the frequency of internal vertices f_i,

$$f_i=\frac{\tau^{-3}}{\tau^4-1}+\tau^{-5}+\tau^{-4}=\frac{3-\tau}{5}\simeq 0.276\,393. \tag{A2}$$

Note that the three frequencies relative to star, boat, and cigar, normalized so that the sum of the three is unity can also be easily deduced from the frequency of Penrose vertex stars.

Star	Boat	Cigar
$\tau^{-4}=\frac{7-4\tau}{\tau+2}=5-3\tau$	$\frac{\tau^2+1}{\tau^5}=\frac{7-4\tau}{\tau}=-11+7\tau$	$\frac{\tau^2+1}{\tau^4}=7-4\tau$

(A3)

2. Some geometrical properties related to deflation inflation

Some useful properties whose proof is elementary are the following.

(1) The external vertices of P are the internal vertices of $D(P)$ (for an illustration, see Fig. 11).

(2) The two most distant vertices of a cigar are the internal vertices of the stars of $D(P)$.

(3) The internal vertices of P are the internal vertices of the stars of $D^2(P)$.

(4) The internal vertices of P are the centers of Penrose vertex stars of type 4 (stars surrounded by fives cigars) of $D^3(P)$.

(5) The internal vertices of P are the centers of stars surrounded by fives boats of $D^4(P)$. (These centers are Penrose vertex stars of type 1 but not all of them.)

[1] R. Penrose, Pentaplexity, Bulletin of the Institute for Mathematics and Applications, **10**, 2 (1974).

[2] M. Senechal, *Quasicrystals and Geometry* (Cambridge University Press, Cambridge, England, 1995).

[3] R. McGrath, J. Ledieu, E. J. Cox, and R. D. Diehl, J. Phys.: Condens. Matter **14**, R119 (2002).

[4] T. C. Choy, Phys. Rev. Lett. **55**, 2915 (1985).

[5] T. Odagaki and D. Nguyen, Phys. Rev. B **33**, 2184 (1986).

[6] M. Kohmoto and B. Sutherland, Phys. Rev. Lett. **56**, 2740 (1986).

[7] M. Kohmoto and B. Sutherland, Phys. Rev. B **34**, 3849 (1986).

[8] B. Sutherland, Phys. Rev. B **34**, 3904 (1986).

[9] M. Marcus, Phys. Rev. B **34**, 5981 (1986).

[10] B. Sutherland, Phys. Rev. B **35**, 9529 (1987).

[11] F. Aguilera-Granja, F. Mejía-Lira, J. L. Morán-López, and R. G. Barrera, Phys. Rev. B **36**, 7342 (1987).

[12] T. Fujiwara, M. Arai, T. Tokihiro, and M. Kohmoto, Phys. Rev. B **37**, 2797 (1988).

[13] M. Holzer, Phys. Rev. B **38**, 1709 (1988).

[14] T. Tokihiro, T. Fujiwara, and M. Arai, Phys. Rev. B **38**, 5981 (1988).

[15] H. Tsunetsugu and K. Ueda, Phys. Rev. B **38**, 10 109 (1988).

[16] M. Krajčí and T. Fujiwara, Phys. Rev. B **38**, 12 903 (1988).

[17] P. Ma and Y. Liu, Phys. Rev. B **39**, 9904 (1989).

[18] S. He and J. D. Maynard, Phys. Rev. Lett. **62**, 1888 (1989).

[19] J. A. Ashraff, J.-M. Luck, and R. B. Stinchcombe, Phys. Rev. B **41**, 4314 (1990).

[20] Y. Liu and P. Ma, Phys. Rev. B **43**, 1378 (1991).

[21] H. Tsunetsugu, T. Fujiwara, K. Ueda, and T. Tokihiro, Phys. Rev. B **43**, 8879 (1991).

[22] H. Tsunetsugu and K. Ueda, Phys. Rev. B **43**, 8892 (1991).

[23] J. Q. You, J. R. Yan, J. X. Zhong, and X. H. Yan, Phys. Rev. B **45**, 7690 (1992).

[24] J. Q. You and F. Nori, J. Phys.: Condens. Matter **5**, 9431 (1993).

[25] G. G. Naumis, R. A. Barrio, and C. Wang, Phys. Rev. B **50**, 9834 (1994).

[26] S. Yamamoto and T. Fujiwara, Phys. Rev. B **51**, 8841 (1995).

[27] G. Kasner, H. Schwabe, and H. Böttger, Phys. Rev. B **51**, 10 454 (1995).

[28] T. Rieth and M. Schreiber, Phys. Rev. B **51**, 15 827 (1995).

[29] S. Roche, G. Trambly de Laissardiére, and D. Mayou, J. Math. Phys. **38**, 1794 (1997).

[30] T. Rieth and M. Schreiber, J. Phys.: Condens. Matter **10**, 783 (1998).

[31] P. Repetowicz, U. Grimm, and M. Schreiber, Phys. Rev. B **58**, 13 482 (1998).

[32] E. S. Zijlstra, A. Fasolino, and T. Janssen, Phys. Rev. B **59**, 302 (1999).
[33] H. Schwabe, G. Kasner, and H. Böttger, Phys. Rev. B **59**, 861 (1999).
[34] G. G. Naumis, J. Phys.: Condens. Matter **11**, 7143 (1999).
[35] E. S. Zijlstra and T. Janssen, Phys. Rev. B **61**, 3377 (2000).
[36] E. S. Zijlstra and T. Janssen, Europhys. Lett. **52**, 578 (2000).
[37] M. Krajčí, J. Hafner, and M. Mihalkowič, Phys. Rev. B **62**, 243 (2000).
[38] D. Schechtman, I. Blech, D. Gratias, and J. W. Cahn, Phys. Rev. Lett. **53**, 1951 (1984).
[39] P. J. Steinhardt and S. Ostlund, *The Physics of Quasicrystals* (World Scientific, Singapore, 1987).
[40] E. de Prunelé and X. Bouju, Phys. Status Solidi B **225**, 95 (2001).
[41] X. Bouju and E. de Prunelé, Phys. Status Solidi B **217**, 819 (2000).
[42] E. de Prunelé, J. Phys. A **30**, 7831 (1997).
[43] P. Roman, *Some Modern Mathemathics for Physicists and Other Outsiders* (Pergamon Press, New York, 1975), Vol. 2.
[44] P. Guyot, P. Kramer, and M de Boissieu, Rep. Prog. Phys. **54**, 1373 (1991).
[45] *Quasicristals: The State of the Art*, edited by D. P. DiVincenzo and P. Steinhardt (World Scientific, Singapore, 1991), p. 447.
[46] L. H. Tang and M. V. Jarić, Phys. Rev. B **41**, 4524 (1990).
[47] C. Robles, www.math.ubc.ca/robles/tiling/penrose/frequencies.html
[48] M. Gardner, Sci. Am. **236**, 110 (1977).
[49] J. Belissard, in *From Number Theory to Physics*, edited by M. Waldschmidt, P. Poussa, J. P. Luck, and C. Itzykson (Springer-Verlag, Berlin, 1992).
[50] J. Kellendonck, Commun. Math. Phys. **187**, 115 (1997).